

Statics Modeling of an Underactuated Wire-Driven Flexible Robotic Arm

Zheng Li, Ruxu Du, Haoyong Yu and Hongliang Ren

Abstract—In this paper, statics model of an underactuated wire-driven flexible robotic arm is introduced. The robotic arm is composed of a serpentine backbone and a set of controlling wires. It has decoupled bending rigidity and axial rigidity, which enables the robot large axial payload capacity. Statics model of the robotic arm is developed using the Newton-Euler method. Combined with the kinematics model, the robotic arm deformation as well as the wire motion needed to control the robotic arm can be obtained. The model is validated by experiments. Results show that, the proposed model can well predict the robotic arm bending curve. Also, the bending curve is not affected by the wire pre-tension. This enables the wire-driven robotic arm with potential applications in minimally invasive surgical operations.

I. INTRODUCTION

Underactuated flexible manipulators (UFM) are of growing interests in recent years, especially in the field of robotic surgery [2-5], industrial inspection [6], underwater propulsion [7-9], etc. In these applications, the manipulator needs be flexible, compact in structure. UFM usually have limited payload ability and limited positioning accuracy. As the number of actuators is much less than the robot DOFs the robot motion or deformation is related to the forces exerted on it. For inspection tasks, the positioning accuracy and payload capacity of the UFM is not crucial. However, for manipulation tasks, e.g. performing a surgery operation, precision positioning is important. Also, the payload capacity of the robotic arm is crucial as there are a lot of operations, e.g. cutting tissues, suturing, etc. How the forces, including the controlling forces and external loads influence the robotic arm deformation is therefore crucial.

In previous work, researchers mainly focus on the design and kinematics of UFM. Some common design approaches include, tendon/wire/cable driven [10] and concentric tube design [3, 4]. Among the few articles discussing UFM statics,

most of them deal with continuum robotic arms [11-15]. The UFM is modeled as a continuous beam, and the statics is based on Bernoulli-Euler Constitutive Law [12-14] or Crossrat Rod Theory [11, 15]. These models well predict the UFM backbone deformation under external loadings, and validations are given with simple loading conditions. For underactuated serpentine robotic arms, the structure is different, hence, above models are not applicable. Also, traditional statics models for fully actuated serpentine robotic arms are not suited to the underactuated ones.

This paper gives the statics model of a wire-driven underactuated serpentine robotic arm, whose design was presented in our previous work [10]. Compared to continuum robotic arms, this type of robotic arm has decoupled axial rigidity and bending rigidity. The statics model of the wire-driven robotic arm is derived from Newton-Euler method. From the model, one can predict the deformed backbone curve when all the forces are known; or calculate the wire tension needed to manipulate the robotic arm distal tip to a desired position with known external loadings. Wire motion can be calculated from the kinematics model.

The rest of the paper is organized as follows: section II presents the underactuated wire-driven flexible robotic arm; section III reviews the kinematics model; section IV shows the statics modeling; section V gives the experimental validation; finally, section VI concludes the paper.

II. WIRE-DRIVEN FLEXIBLE ROBOTIC ARM

The wire-driven flexible robotic arm comprises a number of vertebrae, a couple of wire pairs and several elastic components [10, 16]. The vertebrae are serially linked, with adjacent vertebrae form a joint, either revolute joint or spherical joint. When all the joints are revolute joint, the robotic arm motion is planar bending. It can bend side to side in a plane. Otherwise, if all the joints are spherical joint, the robotic arm motion is spatial. It can bend to all directions. The joint motion is confined by the elastic component, such as an elastic tube. Vertebrae together with the elastic components make up the flexible backbone of the robotic arm. The wire pairs go through all the vertebrae and are fastened to the backbone distal end. The other end of the wires is connected to the actuators.

Figure 1 shows a planar wire-driven flexible robotic arm. It has a base, ten vertebrae, a uniform elastic tube, and a pair of controlling wires. The vertebra length is H and the joint gap distance is h_0 . At resting position, the robotic arm is straight as in Fig. 1 (a). By pulling one wire and releasing the other, the robotic arm bends as in Fig. 1 (b). The robotic arm

Resrach supported by FRC Tier I grants R397000156112 and R397000157112, awarded to H. Yu and H. Ren, National University of Singapore.

Zheng Li is with the Department of Biomedical Engineering, National University of Singapore, Singapore (email: bielizh@nus.edu.sg)

Ruxu Du is with the department of mechanical & automation engineering, the Chinese University of Hong Kong, Hong Kong SAR, China (email: rd@mae.cuhk.edu.hk)

Haoyong Yu is with the Department of Biomedical Engineering, National University of Singapore, Singapore (Phone: (65)-66011590; Fax: (65)-68723069; Email: bieyhy@nus.edu.sg)

Hongliang Ren is with the Department of Biomedical Engineering, National University of Singapore, Singapore (phone: (65)-66012802; email: ren@nus.edu.sg)

Corresponding authors: H. Yu and H. Ren

bending motion can be controlled by one or two actuators. In this design, each joint can bend up to 14.27° , and the bending limit of the robotic arm backbone is 142.7° [10].

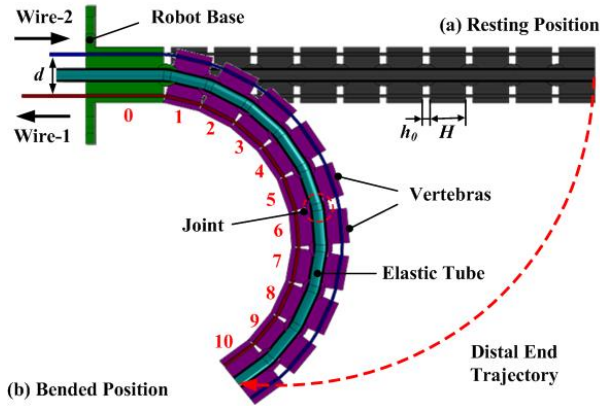


Fig. 1 Planar Wire-Driven Flexible Robotic arm

As shown in the figure, the backbone has two parts. One is the rigid vertebras and the other is the elastic tube. The elastic tube serves as the torsion spring on each joint. It constrains the joints rotations. The tube cross section area is uniform. As a result, the constraint on each joint is the same. On the other hand, the elastic tube deformation is also confined by the vertebras rotations. The tube has two parts, one is attached to the vertebras and the other is in the joints. During the bending, only the second part deforms. When the robotic arm bends, the tube axis is coincident with the robotic arm neutral axis, i.e. the tube length is constant, or the tube deformation is pure bending. With this design, the robotic arm has high axial rigidity and can bend largely.

III. KINEMATICS OF THE ROBOTIC ARM

In wire-driven robotic arm manipulation, the wires control the backbone deformation, or the joints rotations. From the backbone deformation, the distal end position and orientation can then be obtained. Without considering the external load, the deformed backbone shape is assumed a circular arc (constant curvature assumption) [10]. However, different from traditional discrete rigid robotic arm, the wire-driven flexible robotic arm's configuration is affected by the external loads a lot. The constant curvature assumption does not stand when there is an external load. For the wire-driven robotic arm, the kinematics and statics are coupled as in Fig. 2.

The kinematics model of the underactuated wire-driven robotic arm was presented in our previous work, details are in [10, 16, 17]. The kinematics is composed of four parts ($f_1, f_1^{-1}, f_2, f_2^{-1}$) as shown in Fig. 2. In the model, external load was not considered. Considering the external loads, the joints rotations are not identical anymore, the previous kinematic model needs be modified.

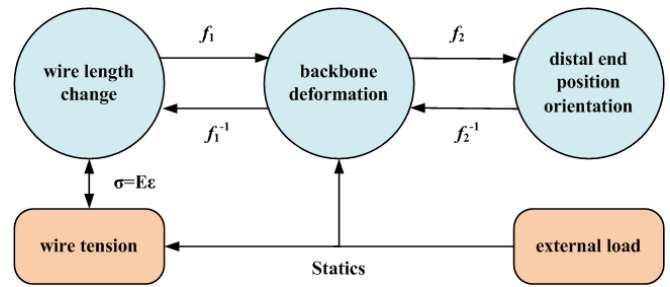


Fig. 2 Coupled Kinematics and Statics

When there is an external load, the backbone deforms differently. The distal end position is only determined by the backbone deformation. Equation (1) shows the relationship. In the equation, θ_i is the rotation of joint i .

$$f_2: \begin{cases} x = \sum_{i=1}^N (H + h_0) \cdot \cos\left(\sum_{j=1}^i \theta_j\right) \\ y = \sum_{i=1}^N (H + h_0) \cdot \sin\left(\sum_{j=1}^i \theta_j\right) \end{cases} \quad (1)$$

The wire length change is determined by the backbone deformation as well as the wire tension. From Fig. 2, the wire length change induced by the tension is: $\Delta L_j = L_j \cdot \varepsilon_j$, $\varepsilon_j = \sigma_j / E$, where E is the Young's Modulus of the wire, ε_j is the strain, σ_j is the stress, and $j=1,2$ is the index of the wires. However, the length change induced by the wire tension is negligible. In this robotic arm, steel wire with 0.5 mm diameter is used. When the pulling force is 10 N, the strain of the wire is 0.024%. Comparing to the length change induced by the wire motion (a few percent), this is negligible. Hence, for some general situation, the wire length can be calculated as per Equation (2). In the equation, L_0 is the initial wire length, and d is the wire spacing distance.

$$f_1^{-1}: \begin{cases} L_1 = L_0 + \sum_{i=1}^N \left[d \cdot \sin\left(\frac{\theta_i}{2}\right) - 2h_0 \cdot \sin^2\left(\frac{\theta_i}{4}\right) \right] \\ L_2 = L_0 - \sum_{i=1}^N \left[d \cdot \sin\left(\frac{\theta_i}{2}\right) + 2h_0 \cdot \sin^2\left(\frac{\theta_i}{4}\right) \right] \end{cases} \quad (2)$$

For the wire-driven robotic arm, the backbone deformation or joints rotations are strongly affected by the external loads. Thus, statics modeling is crucial.

IV. STATICS OF THE ROBOTIC ARM

The planar wire-driven flexible robotic arm is an N -link manipulator with constraints on each joint. In the above design, the link number is ten and a uniform constraint is applied via the elastic tube. Wires are soft and massless. They are ignored in the static analysis.

The forces acted on the robotic arm are divided into two categories. One is the external loads, and the other is the controlling forces from the wires. The loads applied to the backbone can be various, such as distributed force, lumped force, and moment. In calculating the backbone distal end deflection, from the theorem of reciprocal displacements [18], any arbitrary external load is equivalent to a lumped force and a pure moment at the backbone distal end. Hence, in the analysis, only one loading condition is considered, i.e., a

lumped force F_{ex} , a lumped force F_{ey} , and a pure moment M_e are applied to the distal end of the backbone. The backbone bending is actively controlled by the wires. The two wires are equally pretensioned, and the tension is T_p . At the resting position, the resultant controlling force acted on the backbone is an axial force without bending moment. When the two wires change lengths, the tensions in the wires are different [10]. Also, when external loads are applied, the tensions in the wires change. The resultant controlling forces applied to the backbone are a concentrated force $T=T_1+T_2$ and a bending moment M .

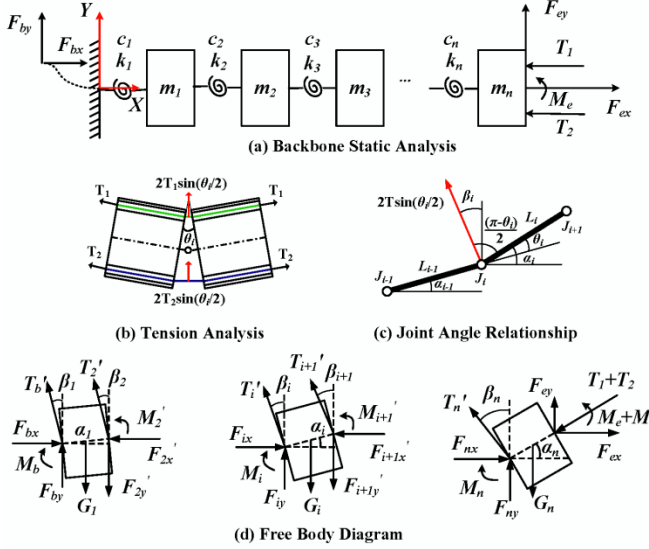


Fig. 3 Static Analysis of Wire-Driven Flexible Robotic arm

In the analysis, the robotic arm is modeled as in Fig. 3 (a). Each vertebra is modeled as a link, and the elastic tube is modeled as a number of spiral springs, the spring constants of all the springs are identical. The coordinate frame is set at the first joint rotation center. The X axis is along the resting position. In the figure, F_{ex} , F_{ey} and M_e are the external loadings, T_1 and T_2 are the wire tensions. When the wires are tensioned, they apply a lateral force T'_i to the vertebrae, as shown in Fig. 3 (b). The lateral force is related to the joint rotation and wire tension. The free body diagrams (FBD) of the vertebrae are shown in Fig. 3 (d). In the figure, F_{bx} , F_{by} and M_b are the forces and moment from the robot base; F_{ix} , F_{iy} , M_i and F_{ix}' , F_{iy}' , M_i' are the forces, moments and their corresponding reactions among the joints. The angles are defined as in Fig. 3 (c). In the figure, J_i denotes the joint i , $L_i = H+h_0$ is the length of link i , θ_i is the joint rotation, α_i is the link orientation in world coordinate frame, β_i is the angle between T'_i and Y axis.

The actuation moment applied via the wires is:

$$M = \Delta T \cdot d = (T_1 - T_2) \cdot d \quad (3)$$

where, d is the wire spacing distance as in Fig. 1.

Assume the Young's modulus of the elastic tube is E , and the second axial moment of area is I_z . For each joint, the rotation is small. Therefore, the torque applied to the joints by

the tube is as per Equation (3). At the first joint, the torque is $M_b = EI_z \cdot \alpha_1 / h_0$.

$$M_i = EI_z \cdot (\alpha_i - \alpha_{i-1}) / h_0, \quad i = 2, 3, \dots, N \quad (4)$$

From the free body diagram, the force balance equations can be found. For the first vertebra, i.e. $i=1$ to $N-1$:

$$\begin{cases} F_{ix} = F_{i+1x}' + T'_i \sin \beta_i + T'_{i+1} \sin \beta_{i+1} \\ F_{iy} = F_{i+1y}' + G_i - T'_i \cos \beta_i - T'_{i+1} \cos \beta_{i+1} \\ M_i = M_{i+1}' + L_i \left[F_{i+1x}' \sin(\alpha_i) - (F_{i+1y}' + 0.5G_i) \cos(\alpha_i) + T'_{i+1} \cos\left(\frac{\theta_{i+1}}{2}\right) \right] \end{cases} \quad (5)$$

When $i=1$, $T'_1 = T'_b$. For the last vertebra, i.e. $i=N$:

$$\begin{cases} F_{nx} = T \cos(\alpha_n) - F_{ex} + T'_n \sin(\beta_n) \\ F_{ny} = T \sin(\alpha_n) - F_{ey} + G_n - T'_n \cos(\beta_n) \\ M_n = M_e + M - L_n \left[F_{ex} \sin(\alpha_n) - (F_{ey} - 0.5G_n) \cos(\alpha_n) \right] \end{cases} \quad (6)$$

where, $\theta_1 = \alpha_1$, $\theta_i = \alpha_i - \alpha_{i-1}$, $\beta_1 = \alpha_1/2$, $\beta_i = (\alpha_i + \alpha_{i-1})/2$, and $T'_i = T \sin(\theta_i/2)$.

From the statics model, when all the external loadings and controlling forces are given, the joints rotations can be obtained. In practice, one may be more concerned about how to manipulate the backbone distal end to a desired position under given loading conditions. In other words, when the distal end position and external loads are given, what the controlling forces, joints rotations and the wire motions are.

Assume the pre-tension of the wires are both T_p , and the robotic arm is pulled by wire-1. From Equation (3) we have:

$$\begin{cases} T_1 = T_p + M/d \\ T_2 = T_p \end{cases} \quad (7)$$

From Equation(1), and Equation (3) to Equation(7), there are $4N+2$ unknowns (T_1 , T_2 , M_i , F_{ix} , F_{iy} , α_i) and $4N+4$ independent equations. The controlling forces can be solved. It is noted that, since the backbone deformation is not affected by axial force, in the solution T_2 is set to T_p . The initial value of the joint rotation can be chosen using the constant curvature assumption. Note that, when all the joints rotations are identical, Eq. (1) can be rewritten as Eq. (8), thus the initial values of link orientation can be chosen as in Eq. (9).

$$\begin{cases} x = \tilde{R} \cdot \cos\left(\frac{N+1}{2}\theta\right) \cdot \sin\left(\frac{N}{2}\theta\right) \\ y = \tilde{R} \cdot \sin\left(\frac{N+1}{2}\theta\right) \cdot \sin\left(\frac{1}{2}\theta\right) \end{cases}, \text{ with } \tilde{R} = (H+h_0) \cdot \sin\left(\frac{1}{2}\theta\right) \quad (8)$$

$$\alpha_{i0} = \frac{2 \cdot i}{N} \cdot \arctan\left(\frac{y}{x}\right) \quad (9)$$

V. EXPERIMENT VALIDATION AND DISCUSSION

To examine the proposed statics model, a wire-driven flexible robotic arm is developed. It has ten vertebrae,

including the base. The length of each vertebra is 12.5 mm, and the joint gap distance is 2.5 mm. The joints can rotate up to 14.25°. The vertebrae are made by 3D printing, and the material is ABS plastic. Each vertebra weight 2.83g. Detailed vertebra information can be found in [10]. An elastic rubber tube is used to confine the joints rotations. The outer diameter is 2.1 mm, and the inner diameter is 2.0 mm. The Young's Modulus of the tube is 1.5 GPa. A pair of 0.5 mm diameter steel wires are used to control the backbone bending. The experiment set up is shown in Fig. 4.

In the experiment, the robotic arm is horizontally suspended by the base. Two wires are guided by the pulleys to control the robotic arm bending. External load is applied via a mass hung at the distal tip. The backbone curve is measured using stereo vision, and the grid paper is used for calibration. Three experiments are carried out. In the first experiment, the robotic arm is controlled without payload; in the second experiment, a vertical payload is applied at the distal end; at last, the influence of wire pre-tension is tested.

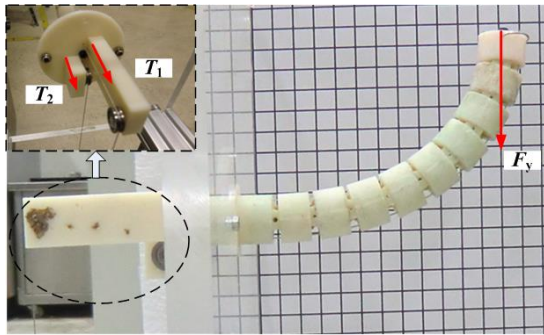


Fig. 4 Experiment Setup

A. Experiment 1 - without external load

In this experiment, the robotic arm is controlled without external loads, i.e. $F_{ex}=0$, $F_{ey}=0$, $M_c=0$. The robotic arm is bent by its own weight and the wires. In the beginning, the pulling forces of the two wires are $T_1=T_2=2$ N. After that, the tension of the upper wire is increased and the tension of the second wire remains constant. Four cases are tested, i.e. 1) $T_1=2$ N, $T_2=2$ N; 2) $T_1=6$ N, $T_2=2$ N; 3) $T_1=7$ N, $T_2=2$ N; 4) $T_1=8$ N, $T_2=2$ N.

The deformations of the backbone are as in Fig. 5. In the figure, the solid curves represent the simulated backbone curve, and the circles are the simulated joint position; the dashed curves denote the measured backbone curves, and the squares are the measured joint position. The results of the four cases are shown by different colors, where red represents for case 1, green represents for case 2; blue represents for case 3; and magenta represents for case 4.

Fig. 6 shows the simulated joint rotations in the four cases. From the figure, when the pulling forces of the two wires are the same ($T_1=2$ N), the backbone deformation is mainly determined by the joints near the base, the last two joints rotations are almost zero. When the pulling force is large as in the cases $T_1=7$ N (blue) and $T_1=8$ N (purple), the distal joints first reach the maximum rotation (overlapped in the figure). This shows when considering the statics, the constant

curvature assumption does not stand any more. Considering equation (2), the length change of the two wires are $\Delta L_1=-2.66$ mm and $\Delta L_2=2.62$ mm respectively. When the pulling force T_1 is increased, the robotic arm is bent upward. The wires length changes in the four cases are: 2) $\Delta L_1=3.24$ mm, $\Delta L_2=-3.35$ mm; 3) $\Delta L_1=10.72$ mm, $\Delta L_2=-11.19$ mm; 4) $\Delta L_1=14.57$ mm, $\Delta L_2=-15.32$ mm. From the results, the statics model can well predict the robotic arm bending in all the cases. Also from the experiments, the wire length changes in all the cases are predicted reasonably well.

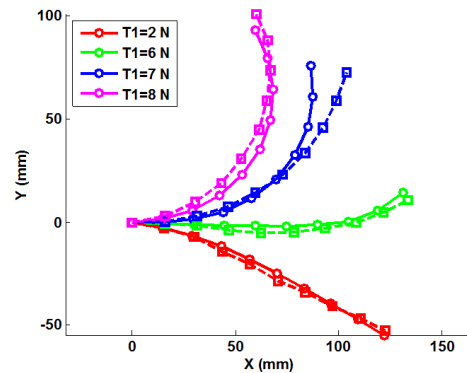


Fig. 5 Backbone Deformation without External Load

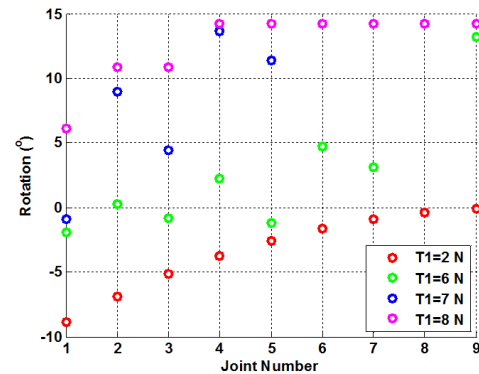


Fig. 6 Simulated Joint Rotation without External Load

B. Experiment 2 – with vertical payload

In this experiment, the robotic arm is controlled to lift a weight vertically. The loading condition is $F_{ex}=0$, $F_{ey}=1$ N, $M_c=0$. The pre-tensions of the wires are the same as in the previous experiment. Three cases are tested, i.e. 1) $T_1=10$ N, $T_2=2$ N; 2) $T_1=11$ N, $T_2=2$ N; 3) $T_1=12$ N, $T_2=2$ N.

The deformations of the backbone is as in Fig. 7. Similarly, the solid curves are the simulated backbone deformation, and the dashed curves are the measured backbone deformation. The results of the three cases are shown by red, green and blue respectively. When there is a vertical payload, the backbone deformation is much different. The deformed backbone curve is S shape, while in the previous experiment, the deformed backbone curves are in C shape. The joints rotations are as shown in Fig. 8. From the figure, when $T_1=12$ N, the first joint reaches its rotation limit, so do the last four joints. This shows

the adjacent vertebrae contact each other. When the pulling force is further increased, the two vertebrae are 'locked together'. The number of rotating vertebrae is then reduced, and the robot bending rigidity is increased.

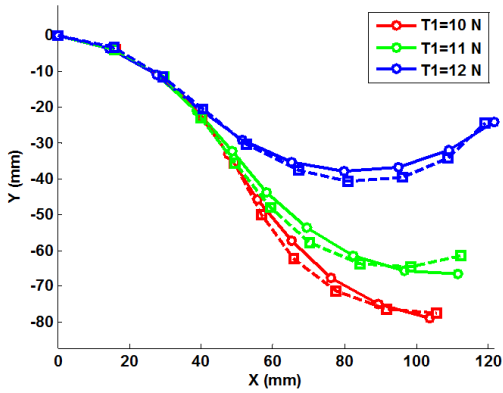


Fig. 7 Backbone Deformation with 1 N Vertical Payload

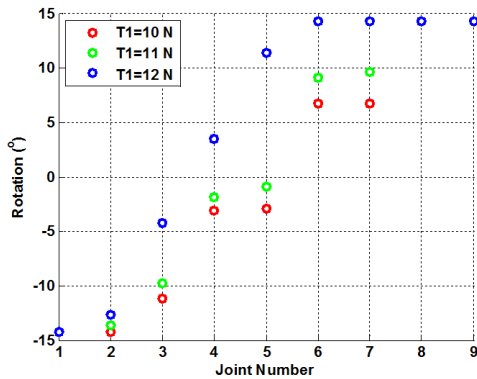


Fig. 8 Simulated Joint Rotation without 1 N Vertical Load

C. Experiment 3 – influence of the wire pre-tension

From the statics model, when the two wires are equally pre-tensioned, the backbone deformation is independent to the magnitude of the pre-tension. This experiment is designed to test this feature. In the experiment, the robotic arm external loading condition is the same as that of experiment 1, i.e. $F_{ex}=0$, $F_{ey}=0$, $M_e=0$. The two wires are equally pretensioned. Five cases are tested: 1) $T_1=T_2=0$ N; 2) $T_1=T_2=1$ N; 3) $T_1=T_2=2$ N; 4) $T_1=T_2=3$ N; 5) $T_1=T_2=4$ N. The measured backbone deformation is shown in Fig. 9.

From the results, the backbone deformations are consistent with some variations. The variation is caused by several factors, including the friction between the joints, friction between the wire and vertebrae, the measurement error, etc. The results show that, the backbone bending is not affected by the magnitude of the wire pre-tension.

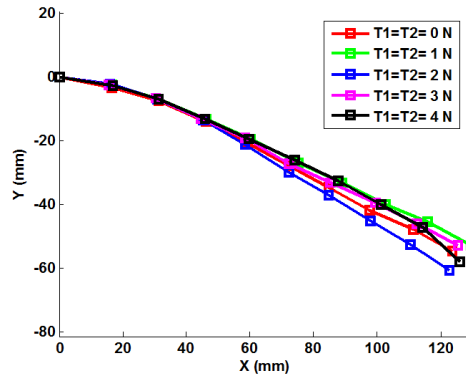


Fig. 9 Backbone Deformation with Different Wire Pre-tension

D. Discussion

In the experiment, the robotic arm backbone deformation under some simple load conditions is tested. The results validate the proposed model. Due to the limitation of the test bed, some other more complicated loading conditions are not tested. Instead, simulations are performed. Fig. 10 shows the robots deformation under five loading conditions.

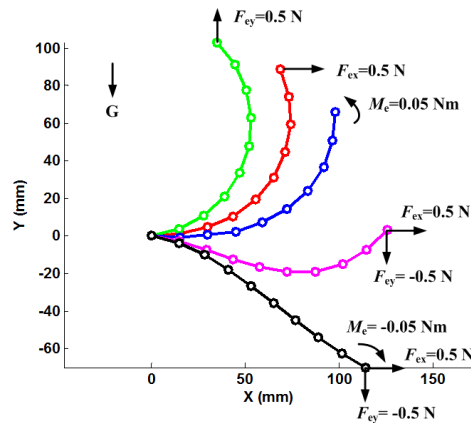


Fig. 10 Simulated Backbone Curve at Different Loading Conditions

- case 1: $T_1=8$ N; $T_2=2$ N; $F_{ex}=0.5$ N; $F_{ey}=0$ N; $M_e=0$ Nm
- case 2: $T_1=8$ N; $T_2=2$ N; $F_{ex}=0$ N; $F_{ey}=0.5$ N; $M_e=0$ Nm
- case 3: $T_1=8$ N; $T_2=2$ N; $F_{ex}=0$ N; $F_{ey}=0$ N; $M_e=0.05$ Nm
- case 4: $T_1=8$ N; $T_2=2$ N; $F_{ex}=0.5$ N; $F_{ey}=-0.5$ N; $M_e=0$ Nm
- case 5: $T_1=8$ N; $T_2=2$ N; $F_{ex}=0.5$ N; $F_{ey}=-0.5$ N; $M_e=-0.05$ Nm

From the results, the backbone bending curve is smooth. The force in +Y direction and a positive bending moment tends to bend the backbone as in case 2) and 3). The backbone bending is very sensitive to the vertical force and bending moment. From case 1) and case 4) when there is an additional vertical force, the backbone deformation is very different: the robotic arm is straightened a lot. From case 4) and case 5), with a negative bending moment, the robotic arm is further straightened from case 2). All of these show that the wire-driven flexible robotic arm is sensitive to the loads other than axial direction.

From experiment 3, the wire-driven flexible robotic arm deformation is independent on the magnitude of the wire

pre-tension. This shows the decoupled rigidity of the wire-driven flexible robotic arm. The robot can bear large payload in axial direction. This is especially useful for some applications, such as cutting tissues with scissors. The cutting forces are symmetric, and can be transferred to the axial direction. As a result, the wire-driven flexible robotic arm can be used in cutting hard tissues. For current flexible robots, e.g. concentric tube robots or tendon-driven robots, the rigidity in bending direction and axial direction are both low. This limits the payload capability of the robots, and constrains their applications.

From the experiments, it is observed that the influence of the friction cannot be ignored. Although, lubricant grease is used, at some configurations, the robotic arm is not sensitive to the actuation force. This shows the static friction needs be included in the statics model. Also, the contacting of two vertebrae need be considered in the statics model. These will be considered in the future work.

VI. CONCLUSION

This paper presents an underactuated wire-driven flexible robotic arm and its statics model. The robotic arm has a large number of joints, whose motion is controlled by a pair of wires. It is flexible, and highly underactuated. The robotic arm deformation is not only dependent on the actuation, but also the external loads. The kinematics and statics are coupled together. The axial rigidity and bending rigidity of the robotic arm are decoupled. This improves the payload capability in axial direction. It is modeled as an N -link manipulator with a spiral spring on each joint. From the model, when all the external loadings and controlling forces are known, the robotic arm deformation can be calculated. Also, the required wire motion and controlling forces to manipulate the robotic arm distal end to a desired position with given external loading conditions can be predicted. The model is validated by experiments. Incorporating instrument tracking and navigation capabilities [19-22], the proposed flexible robotic system are expected to be applied to robotic surgeries.

REFERENCES

- [1] H. Ren, C. M. Lim, J. Wang, W. Liu, S. Song, Z. Li, G. Herbert, Z. Tse & Z. Tan "Computer Assisted Transoral Surgery with Flexible Robotics and Navigation Technologies: A Review of Recent Progress and Research Challenges" *Critical Reviews in Biomedical Engineering*, Begel House Inc., 2014
- [2] T. Fisher, A. Hamed, P. Vartholomeos, K. Masamune, G. Tang, H. Ren & Z. T. H. Tse "Intraoperative magnetic resonance imaging—conditional robotic devices for therapy and diagnosis" *Proceedings of the Institution of Mechanical Engineers, Part H: Journal of Engineering in Medicine*, 2014.
- [3] P. Dupont, A. Gosline, N. Vasilyev, J. Lock, E. Butler, C. Folk, A. Cohen, R. Chen, G. Schmitz, H. Ren & P. del Nido "Concentric Tube Robots for Minimally Invasive Surgery" *Hamlyn Symposium on Medical Robotics*, 2012, 7, 8.
- [4] P. E. Dupont, J. Lock, B. Itkowitz, and E. Butler, "Design and Control of Concentric-Tube Robots," *IEEE Transactions on Robotics*, vol. 26, pp. 209-225, Apr 2010.
- [5] Y. Zhou, H. Ren, M. Q.-H. Meng, Z. T. H. Tse & H. Yu "Robotics in Natural Orifice Transluminal Endoscopic

- Surgery" *Journal of Mechanics in Medicine and Biology*, World Scientific, 2013, 13, 1350044.
- [6] *Snake Arm*. Available: <http://www.ocrobotics.com/>
- [7] Z. Li and R. Du, "Design and analysis of a biomimetic wire-driven flapping propeller," in *Biomedical Robotics and Biomechanics (BioRob), 2012 4th IEEE RAS & EMBS International Conference on*, 2012, pp. 276-281.
- [8] Z. Li, W. Gao, R. Du, and B. Liao, "Design and Analysis of a Wire-Driven Robot Tadpole," in *International Mechanical Engineering Congress & Exposition (IMECE 2012)*, Houston, Texas, USA, 2012.
- [9] B. Liao, Z. Li, and R. Du, "Robot Tadpole with a Novel Biomimetic Wire-driven Propulsor," presented at the IEEE International Conference on Robotics and Biomimetics (ROBIO 2012), Guang Zhou, China, 2012.
- [10] Z. Li, R. Du, M. C. Lei, and S. M. Yuan, "Design and Analysis of a Biomimetic Wire-Driven Robot Arm," in *Proceedings of the ASME 2011 International Mechanical Engineering Congress & Exposition*, 2011, pp. 11-17.
- [11] B. A. Jones, R. L. Gray, and K. Turlapati, "Three dimensional statics for continuum robotics," in *Intelligent Robots and Systems, 2009. IROS 2009. IEEE/RSJ International Conference on*, 2009, pp. 2659-2664.
- [12] D. C. Rucker, B. A. Jones, and R. Webster, "A model for concentric tube continuum robots under applied wrenches," in *2010 IEEE International Conference on Robotics and Automation (ICRA)* Anchorage, Alaska, USA, 2010, pp. 1047-1052.
- [13] D. B. Camarillo, C. F. Milne, C. R. Carlson, M. R. Zinn, and J. K. Salisbury, "Mechanics modeling of tendon-driven continuum manipulators," *Robotics, IEEE Transactions on*, vol. 24, pp. 1262-1273, 2008.
- [14] J. Lock, G. Laing, M. Mahvash, and P. E. Dupont, "Quasistatic modeling of concentric tube robots with external loads," in *Intelligent Robots and Systems (IROS), 2010 IEEE/RSJ International Conference on*, 2010, pp. 2325-2332.
- [15] D. C. Rucker and R. J. Webster, "Statics and dynamics of continuum robots with general tendon routing and external loading," *Robotics, IEEE Transactions on*, vol. 27, pp. 1033-1044, 2011.
- [16] Z. Li and R. Du, "Design and Analysis of a Bio-Inspired Wire-Driven Multi-Section Flexible Robot," *Int J Adv Robotic Sy*, vol. 10, 2013.
- [17] Z. Li and R. Du, "Design and implementation of a biomimetic wire-driven underactuated serpentine manipulator," *Transaction on Control and Mechanical Systems*, vol. 1, pp. 250-258, 2012.
- [18] A. F. Bower, *Applied Mechanics of Solids*: CRC Press, 2009.
- [19] H. Ren, E. Campos-Nanez, Z. Yaniv, F. Banovac, N. Hata & K. Cleary "Treatment Planning and Image Guidance for Radiofrequency Ablations of Large Tumors" *IEEE Transactions on Information Technology in Biomedicine (IEEE Journal of Biomedical and Health Informatics)*, 2013.
- [20] S. Song, W. Qiao, B. Li, C. Hu, H. Ren & M.-H. Meng "An Efficient Magnetic Tracking Method Using Uniaxial Sensing Coil" *IEEE Transactions on Magnetics*, IEEE, 2014, 50, 1-7
- [21] H. Ren, W. LIU & A. LIM "Marker-Based Instrument Tracking Using Dual Kinect Sensors for Navigated Surgery" *IEEE Transactions on Automation Science and Engineering*, 2013.
- [22] H. Ren & P. Kazanzides "Investigation of Attitude Tracking Using an Integrated Inertial and Magnetic Navigation System for Hand-Held Surgical Instruments" *IEEE/ASME Transactions on Mechatronics*, 2012, 17, 210 -217